On the Limit Analysis of Soil and Rock Foundations Including the Effect of Tensile Cracking

*Norio TAKEUCHI**

1. INTRODUCTION

The finite element method was developed by structural engineers in aerospace industries and made remarkable progress with the advancement of the computer industry [1]. It has become one of the most useful tools for structural analysis and also has been used for analysis of soil and rock foundation structures.

To consider the soil and rock materials as continua they are generally too nonuniform, inhomogeneous and too easy to slip internally under applied loading. On the other hand, granular materials' influence on crack initiation due to tensile load should not be neglected. Therefore, in the case of stability analysis of foundations, it is necessary to consider two failure patterns. One is slip failure, and the other is tensile cracking, including contact problems.

The finite element method, however, treats the soil and rock foundations as continuous materials. GOODMAN developed the joint element to be inserted between constant strain elements in which the effect of discontinuity is taken into account [2]. For finite element analysis of reinforced concrete structures, NGO and others proposed a similar element that is called the linkage element [3]. In the past some work has been carried out along this line[4] [5]. According to these methods it may be possible to obtain reasonable results for the problems where discontinuous surfaces are prescribed. In real soil and rock foundations, such discontinuous faces are not a priori known and therefore application of this method may be limited.

On the other hand, Prof. KAWAI proposed a family of new discrete models in 1976 based on experimental evidence on the flow and fracture of solids [6]. In these models structures or solids are idealized as a set of rigid elements interconnected by two types of spring systems, one of which resists the dilatational deformation, the other, the shearing deformation. Therefore sliding or separation of two adjacent elements can be calculated easily.

Formerly, the author individually analyzed slip failure and tensile cracking in stability problems of foundations, using the Rigid Bodies-Spring Model (RBSM).

*理工学部土木工学科助教授　計算力学・応用力学

However, coupled failure may be generated in the foundations. Therefore, we developed a new algorithm which may be applicable in analysing the coupled failure of solids due to slipage, tensile cracking and solid contact.

In this paper, the theoretical basis of this algorithm is described first, and then the applicability of the method to the stability problems of foundations is discussed.

2. FORMULATION OF A TWO DIMENSIONAL RBSM

For explaining the formulation of a two dimensional RBSM, we considered two rigid triangular elements as shown in Fig.1. Of course, an arbitrary polygon or circle can be used instead of a triangular element. They are assumed to be in equilibrium with external loads and reaction forces of the spring system which are distributed over the contact surface of two adjacent bodies.

The rigid displacement field is assumed in each element, whose nodal displacements are given by the displacement (u, v, θ) of the centroid as shown in Fig.1. Horizontal and vertical displacement U, V at the arbitrary point P can be shown by the following equations :

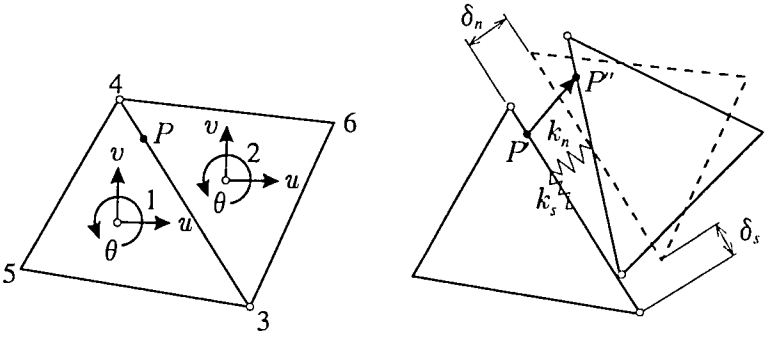

Fig.1 Two dimensional rigid triangular element

$$\boldsymbol{U}=\boldsymbol{Q}\cdot\boldsymbol{u}_i \tag{1}$$

$$\boldsymbol{U}=\{U_I, V_I; U_{II}, V_{II}\}^t$$

$$\boldsymbol{u}_i=\{u_1, v_1, \theta_1; u_2, v_2, \theta_2\}^t$$

$$\boldsymbol{Q}=\left[\begin{array}{ccc:ccc} 1 & 0 & -(y-y_1) & 0 & 0 & 0 \\ 0 & 1 & (x-x_1) & 0 & 0 & 0 \\ \hdashline 0 & 0 & 0 & 1 & 0 & -(y-y_2) \\ 0 & 0 & 0 & 0 & 1 & (x-x_2) \end{array}\right]$$

where subscript I, II or 1, 2 indicate element number 1 or 2, respectively. (x_1, y_1) and (x_2, y_2) are the coordinate values of the centroid for each element.

The relation of the displacement between the global coordinate system and the

local coordinate system along the side $\overline{34}$ of the triangular element is derived by the following matrix equation :

$$\overline{U}=R\cdot U \tag{2}$$

$$\overline{U}=\{\overline{U}_I,\overline{V}_I;\overline{U}_II,\overline{V}_II\}^t \qquad R=\left[\begin{array}{cc:cc} l_1 & m_1 & 0 & 0 \\ l_2 & m_2 & 0 & 0 \\ \hdashline 0 & 0 & l_1 & m_1 \\ 0 & 0 & l_2 & m_2 \end{array}\right]$$

$$l_1=\cos(\overline{x},x)=y_{43}/l_{34}$$
$$l_2=\cos(\overline{x},y)=x_{43}/l_{34}$$
$$m_1=\cos(\overline{y},x)=x_{34}/l_{34}$$
$$m_2=\cos(\overline{y},y)=y_{43}/l_{34}$$

where l_{34} is the length of side $\overline{34}$, $x_{ij}=x_i-x_j$, the superscript (-) indicates the local coordinate system and **R** is a coordinate transformation matrix.

Using these displacements (U, V) with the local coordinate system, the relative displacement vector δ of the point P can be derived as follows :

$$\delta=M\cdot\overline{U} \tag{3}$$

$$\delta=\{\delta_n,\delta_s\}^t \qquad M=\left[\begin{array}{cc:cc} -1 & 0 & 1 & 0 \\ 0 & -1 & 0 & 1 \end{array}\right]$$

Therefore, substituting eq.(1) and eq.(2) into eq.(3), the following relation with the rigid displacement field is easily obtained :

$$\delta=M\cdot R\cdot Q\cdot u_i=B\cdot u_i \qquad (B=M\cdot R\cdot Q) \tag{4}$$

$$B=\left[\begin{array}{cc:cc:cc} -l_1 & -m_1 & l_1(y-y_1)-m_1(x-x_1) & l_1 & m_1 & -l_1(y-y_2)+m_1(x-x_2) \\ \hdashline -l_2 & -m_2 & l_2(y-y_1)-m_2(x-x_1) & l_2 & m_2 & -l_2(y-y_2)+m_2(x-x_2) \end{array}\right]$$

The spring constants k_n and k_s which resist normal and tangential force respectively on the contact surface between element I and element II can be determined systematically by using the finite difference equation for strain components as follows :

$$\varepsilon=\begin{Bmatrix}\varepsilon_n\\ \gamma_s\end{Bmatrix}=\frac{1}{h_1+h_2}\begin{Bmatrix}\delta_n\\ \delta_s\end{Bmatrix}=\frac{1}{h}\delta \tag{5}$$

where $h = h_1+h_2$ is the projected length of a vector connecting centroids along the line perpendicular to $\overline{AC}$, as shown in Fig.2.

On the contact surface $\overline{AC}$ shown in Fig.2, the normal and tangential stresses σ_n, τ_s satisfy the following equations :

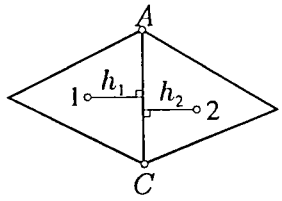

Fig.2 Definition of the projected length

$$\sigma_n=\frac{(1-\nu)E}{(1-2\nu)(1+\nu)}\varepsilon_n \quad , \quad \tau_s=\frac{E}{(1+\nu)}\gamma_s \tag{6}$$

Substituting eq.(5) into eq.(6), the following relation can be obtained :

$$\left.\begin{aligned}\sigma_n&=\frac{(1-\nu)E}{(1-2\nu)(1+\nu)}\cdot\frac{\delta_n}{h_1+h_2}\\ \tau_s&=\frac{E}{(1+\nu)}\cdot\frac{\delta_s}{h_1+h_2}\end{aligned}\right\} \tag{7}$$

On the other hand, from the definition of the spring constants, the following relations are obtained :

$$\sigma_n=k_n\cdot\delta_n \quad , \quad \tau_s=k_s\cdot\delta_s \tag{8}$$

Therefore, comparing equations (7) and (8), the following spring constants can be assumed :

$$\left.\begin{aligned}k_n&=\frac{(1-\nu)E}{(1-2\nu)(1+\nu)(h_1+h_2)}\\ k_s&=\frac{E}{(1+\nu)(h_1+h_2)}\end{aligned}\right\} \tag{9}$$

From eq.(9) the stress-relative displacement relation is derived by the following matrix equation :

$$\boldsymbol{\sigma}=\boldsymbol{D}\cdot\boldsymbol{\delta} \tag{10}$$

$$\boldsymbol{\sigma}=\{\sigma_n,\tau_s\}^t \qquad \boldsymbol{D}=\begin{bmatrix}k_n & 0\\ 0 & k_s\end{bmatrix}$$

$$\boldsymbol{\delta}=\{\delta_n\delta_s\}^t$$

Based on the above preliminaries, the strain energy expression of the in-plane element V can be obtained as the following matrix equation :

$$V=\frac{1}{2}\int_{l_{35}}\delta^t\cdot D\cdot\delta ds=\frac{1}{2}u_i^t\int_{l_{35}}(B^t\cdot D\cdot B)ds\cdot u_i \tag{11}$$

Applying Castigliano's theorem to eq. (11) the following stiffness equation can be derived :

$$\frac{\partial V}{\partial u}=K\cdot u=P \tag{12}$$

where K is a (6×6) symmetric matrix and P is a nodal load vector defined by the following equation :

$$P=\{X_1\ Y_1, M_1; X_2\ Y_2 M_2\}^t \tag{13}$$

3. CONSTITUTIVE LAW FOR THE DISCRETE LIMIT ANALYSIS

In the RBSM, the author considered that reaction stresses are not tensor but vector, and consequently Coulomb's condition may be the most realistic constitutive law for such a discrete system representing granular materials. As is well known, Coulomb's condition can be represented by two straight lines which relate the normal stress σ_n and the shearing stress τ_s. The yield condition of soil-like materials can be modified as shown in Fig.3.

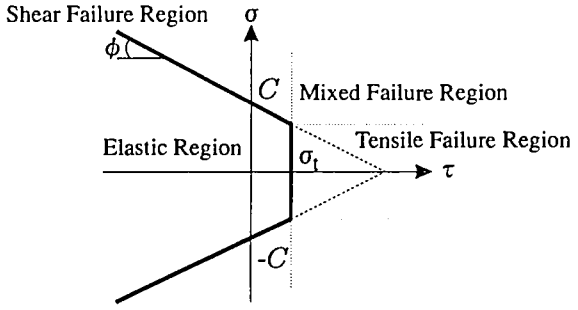

Fig.3 Modified Coulomb's condition where the tensile failure is considered

If σ_n reaches σ_t, σ cannot become greater than this value and therefore the relation between normal stress and strain can be shown as in Fig.4 (a). This is the state of tensile yielding. In the case of granular materials like soils, it is commonly observed that σ is relieved as soon as it reaches σ_t as shown in Fig.4 (b). In this paper a new algorithm is proposed by assuming the spring characteristic as shown in Fig.4 (b) under tensile failure.

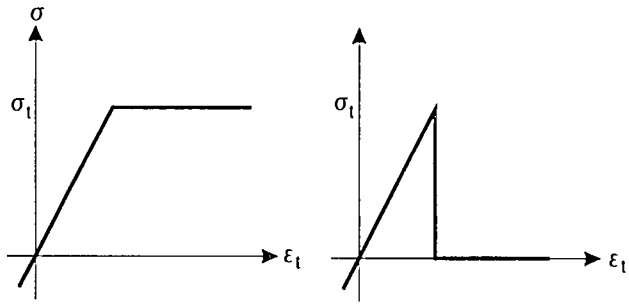

Fig.4 Stress-strain relation at the tensile failure

On the other hand, for determination of spring constants in shear failure, the ordinary plastic flow rule is adopted. It is assumed that plastic yielding will occur if stresses in these spring systems satisfy the following condition :

$$f(\sigma)=0 \tag{14}$$

where $f(\sigma)$ is the yield function in the flow theory of plasticity.

Based on the associated flow rule in which yield function f is equal to plastic potential Q, the relation between stress increments $\Delta\sigma$ and strain increment $\Delta\varepsilon$ can be finally obtained in the following form :

$$\Delta\sigma=\left(D^{(e)}-\frac{D^{(e)}\frac{\partial f}{\partial\sigma}\frac{\partial Q}{\partial\sigma}D^{(e)}}{\frac{\partial f}{\partial\sigma}D^{(e)}\frac{\partial Q}{\partial\sigma}}\right)\Delta\varepsilon \tag{15}$$

where D is the spring matrix and superscript (e) indicates the status of elasticity. Therefore, the plastic spring matrix can be obtained as follows :

$$k_{ij}^{(p)}=k_i^{(e)}\delta_{ij}-\frac{1}{\sum k_i^{(e)}\overline{f}_i^{\,2}}\overline{f_i f_j}k_i^{(e)}k_j^{(e)}$$

$$f_i=\frac{\partial f}{\partial\sigma_i},\quad \sigma_i=(\sigma_n,\tau_s) \tag{16}$$

where $k_{ij}^{(e)}$ is the elastic spring constant and $k_i^{(e)}$ is the diagonal term of the spring matrix.

4. A PROPOSED ALGORITHM FOR NONLINEAR ANALYSIS

A new algorithm is proposed by applying the incremental load procedure developed by YAMADA [7] for the nonlinear problem of soil foundations whose fail-

ure condition is described in the preceding section. In this method (Rmin method), the rate of load increment to yield the most heavily stressed element can be calculated by stress distribution and load increment at the present stage as shown in Fig.5.

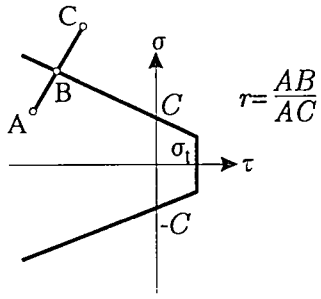

Fig.5 Rate of load increment in the case of shear failure

In this figure, point A represents the stress condition at the previous step, while point C signifies the stress state at the present step. However, the stress equilibrium actually cannot go to point C but must stop at point B on the failure curve. In this condition the required rate of load increment r can be calculated. Once the stress point lies on the failure curve, it may move according to the plastic flow rule until the unloading occurs.

A similar calculation must be made for tensile failure as shown in Fig.6. Point B represents the tensile strength in this figure. When the stresses exceed the tensile strength, the stresses should be reduced to the level corresponding to point B using this rate of stress increment. And then stress (σ_t) must be relieved in that element as shown in Fig.4 (b). Following this operation, both normal and shear springs should be cut to prevent the stress transfer through a common boundary until recontact of these elements occurs.

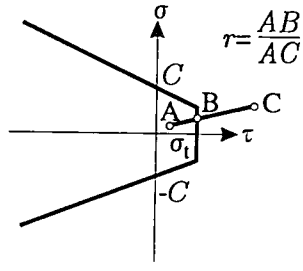

Fig.6 Rate of load increment in the case of tensile failure

All of the possible rate of load increments corresponding to the failure patterns should be calculated in all of the elements, and the minimum rate of load

increment must be determined at each step.

The stress relaxation is usually followed by tensile failure. If the load incremental method is applied to the stress relaxation process exactly, endless calculation should be repeated corresponding to the tensile failure which may occur continuously. Therefore, a supplement of the operation as shown in Fig.7 is to be considered in the iteration at the present loading step.

The load $\boldsymbol{P}^{(i+1)}$ at the $(i+1)$ th step can be calculated by using the load $\boldsymbol{P}^{(i)}$ and the rate of load increment r_i at the present step (i) as follows :

$$\boldsymbol{P}^{(i+1)}=(1-r_i)\boldsymbol{P}^{(i)} \tag{17}$$

Therefore, in the case of shearing failure, residual load $\boldsymbol{P}^{(n)}$ at the nth step can be obtained by using initial load $\boldsymbol{P}$ as follows :

$$\boldsymbol{P}^{(n)}=\prod_{i=0}^{n-1}[1-r_i]\,\boldsymbol{P} \qquad (r_0=0) \tag{18}$$

On the other hand, if crack initiation will cause stress relaxation, relieved forces are taken into account in eq.(18) as follows :

$$\boldsymbol{P}^{(n)}=\prod_{i=0}^{n-1}[1-r_i]\;\boldsymbol{P}+\sum_{k=1}^{n}\Big(\sum_{i=k}^{n}[1-r_i]\,\boldsymbol{F}^{(k-1)}\Big) \tag{19}$$

where $\boldsymbol{F}^{(k)}$ is the relieved force at the kth step.

Here r_{TOTAL} implies the cumulative rate of load increment and it can be defined as follows :

$$r_{TOTAL}=\sum_{k=1}^{n}\Big(\sum_{i=0}^{k-1}[1-r_i]\Big)r_k \tag{20}$$

The calculation must be repeated until $r_{TOTAL}=1$ in each stage of loading.

The rate of load increment specified before calculation may change due to stress relaxation caused by crack initiation. Therefore in this case the concept of r_{TOTAL} may not be correct, but the process of progressive failure may be observed. If $r_{TOTAL}=1$ is realized, however, the iteration must be stopped and the result of the calculation may be considered reliable.

5. NUMERICAL EXAMPLE

As a numerical example, the behavior of an anchor block in the soil foundation subjected to a horizontal force is studied. As shown in Fig.7 (a) tensile stress may be induced in the rear vertical wall of a given block and a cavity may be produced due to tensile cracking as shown in Fig.7 (b)

(a) before deformation (b)after deformation

Fig.7 Anchor block subjected to horizontal force

Fig.8 shows the numerical model and material constants used. In the present analysis, the effect of the gravitational load was neglected.

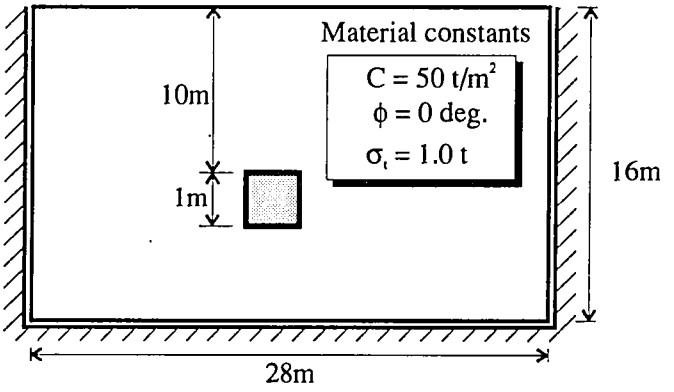

Fig.8 Numerical model and material constants

Fig.9 shows the pattern of the mesh division. The number of the nodes and elements were 234 and 454 respectively, and the total numbers of the interelement springs and degrees of freedom were 657 and 1362 respectively.

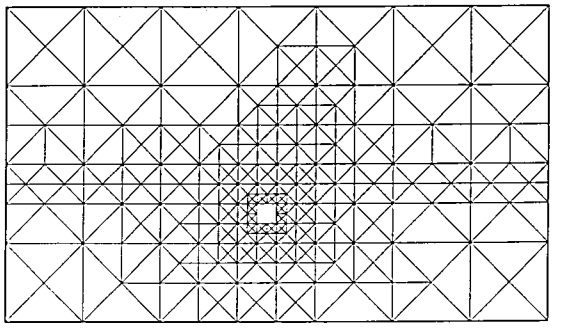

Fig.9 Mesh division

Fig.10 shows the pattern of slip line development in the solution obtained

using discrete limit analysis without the effects of tensile cracking at P=79.7t. As will be seen in the figure, the slip lines were developed on the rear wall of a given block and it is not considered a realistic scenario. Fig.11 shows the displacement pattern from which it can be clearly seen that the soil behind the block was stretched by the block. Actually the soil must separate from the concrete block and it can be concluded that only the previous slip failure analysis, without tensile cracking, cannot present a realistic solution.

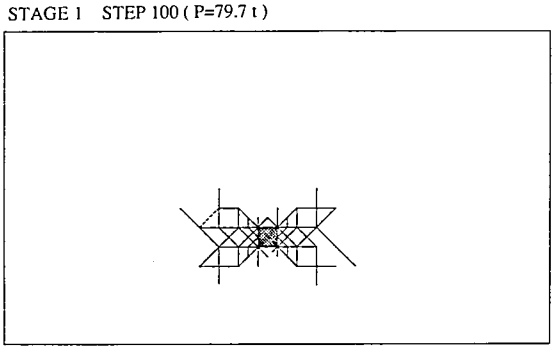

Fig.10 Slip line pattern without the effect of tensile failure

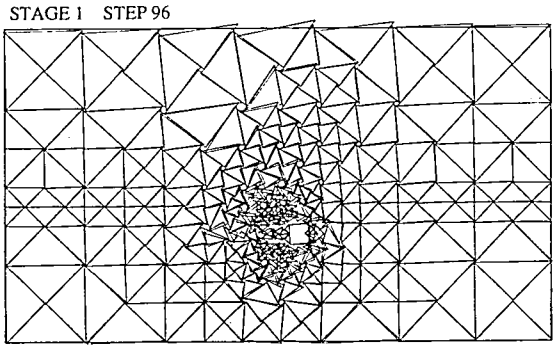

Fig.11 Displacement pattern without the effect of tensile failure

On the other hand, Fig.12 shows patterns of slip development where the effect of tensile failure is considered. In this figure it can be seen that not only slip lines but also tensile cracking may spread on the front region of a given block and the displacement mode may be considerably different from that of the previous solution. The load was applied in a step by step manner, taking the increments as 10t, 10t, 5t, 5t and 5t. Fig.12 shows the slip line pattern of the solution at step 5.

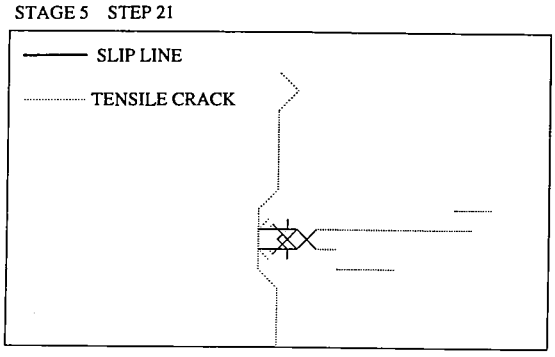

Fig.12 Slip line pattern

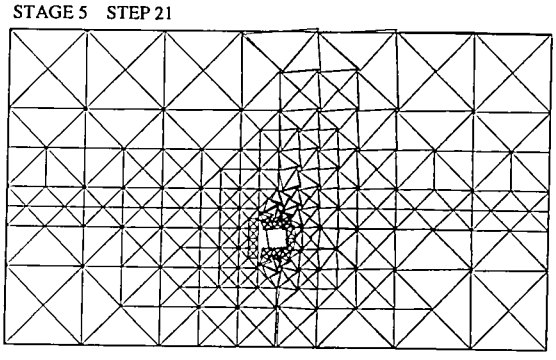

Fig.13 Displacement mode

The failure mode and displacement field corresponding to this step are shown in Fig.13 and Fig.14, respectively. From this figure, separation of the soil on the rear wall of the block and rise of the displacement field near the front wall can be seen.

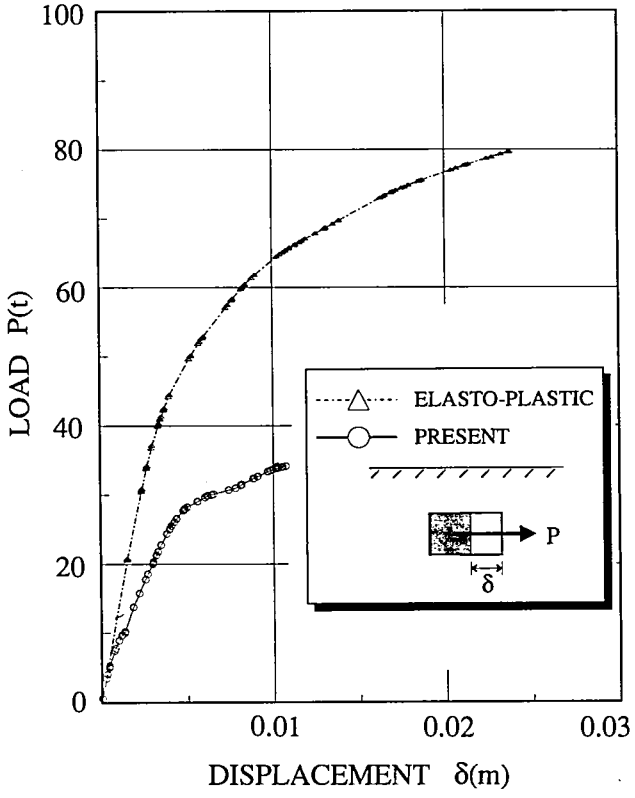

Fig.14 Load-displacement curve

Finally the load - displacement relationship is given in Fig.14. It can be seen from this figure that the displacement corresponding to the latter solution is greater than that of the former, while the load is smaller.

6. CONCLUSION

A new algorithm was developed by which coupled failure due to shear and tensile loads can be treated. Although a numerical example is very simple, it is believed that the present method may be useful in failure analysis of various structural problems in many other fields.

It can be concluded that, comparing this simulation technique with the previous solution procedure, the number of 'if' sentences may increase resulting in time-consuming calculation, but a more realistic analysis can be expected.

REFERENCES

[1] Ziekiewicz,O.C. : The Finite Element Method, Third Edition, McGraw Hill Book Co. (UK) Limited.,1977

[2] Goodman,R.E. : Methods of Geological Engineering of Discontinuous Rock, West

Publishing,1976
[3] Ngo,D. and Scordelis,A.C. : Finite element analysis of reinforced concrete beams, J. of ACI,64,3,pp152-153,1967
[4] Kawamoto,T. and Takeda,N. : An analysis of progressive failure in rock slope, 3rd Int. Conf. on Num. Math. in Geomechanics, Aachen,2-6,Aprill,1979
[5] Cundall,P.A. and Strack,O.D.L. : A discrete numerical model for granular assemblies, Geotechnique,29,1,pp47-65,1979
[6] Kawai,T. : New element models in discrete structural analysis, J. of the Society of Naval Architects of Japan,No.141,pp187-193,1977
[7] Yamada,Y., Yoshimura,N. and Sakurai,T. : Plastic stress-strain matrix and its application for the solution of elasto-plastic problems by the finite element method, Int. J. Mechanical Science,Vol.10, pp343-354,1968